The Astrophysical Journal Letters, 835:L19 (6pp), 2017 February 1 doi:10.3847/2041-8213/835/2/L19

Dynamics of Subarcsecond Bright Dots in the Transition Region above Sunspots and Their Relation to Penumbral Micro-jets

Tanmoy Samanta[1], Hui Tian[2], Dipankar Banerjee[1,3], and Nicole Schanche[4]
[1] Indian Institute of Astrophysics, Koramangala, Bangalore 560034, India; tsamanta@iiap.res.in
[2] School of Earth and Space Sciences, Peking University, China; huitian@pku.edu.cn
[3] Center of Excellence in Space Sciences, IISER Kolkata, India; dipu@iiap.res.in
[4] University of St. Andrews, St. Andrews, UK; ns81@st-andrews.ac.uk
Received 2016 November 10; revised 2016 December 21; accepted 2017 January 10; published 2017 January 25

Abstract

Recent high-resolution observations have revealed that subarcsecond bright dots (BDs) with sub-minute lifetimes appear ubiquitously in the transition region (TR) above sunspot penumbra. The presence of penumbral micro-jets (PMJs) in the chromosphere was previously reported. It was proposed that both the PMJs and BDs are formed due to a magnetic reconnection process and may play an important role in heating of the penumbra. Using simultaneous observations of the chromosphere from the Solar Optical Telescope (SOT) on board *Hinode* and observations of the TR from the *Interface Region Imaging Spectrograph*, we study the dynamics of BDs and their relation to PMJs. We find two types of BDs, one that is related to PMJs, and another that does not show any visible dynamics in the SOT Ca II H images. From a statistical analysis we show that these two types have different properties. The BDs that are related to PMJs always appear at the top of the PMJs, the vast majority of which show inward motion and originate before the generation of the PMJs. These results may indicate that the reconnection occurs at the lower coronal/TR height and initiates PMJs at the chromosphere. This formation mechanism is in contrast with the formation of PMJs by reconnection in the (upper) photosphere between differently inclined fields.

Key words: Sun: corona – Sun: magnetic fields – Sun: oscillations – Sun: transition region – Sun: UV radiation

Supporting material: animations

1. Introduction

Sunspots are regions of concentrated strong magnetic fields comprising a dark central region of umbra surrounded by a less dark region called the penumbra. Penumbral micro-jets (PMJs) are one of the prominent fine-structure dynamical features observed in the sunspot at chromospheric heights. Using Solar Optical Telescope (SOT; Tsuneta et al. 2008) Ca II H filter images, Katsukawa et al. (2007) first reported that these micro-jets occur ubiquitously above penumbra. They have lengths of 1–4 Mm and lifetimes of up to a minute. They generally move very fast and have apparent speeds over 100 km s^{-1}. The magnetic field in the penumbral region consists of a combination of spines (more vertical fields) and interspines (more horizontal fields) (Lites et al. 1993; Bellot Rubio et al. 2004; Scharmer et al. 2011; Scharmer & Henriques 2012; Henriques & Kiselman 2013; Tiwari et al. 2013, 2015). Katsukawa et al. (2007) found that PMJs generally originate near the bright structures in between two dark penumbral filaments and propagate upward along the direction of the spine. This, they proposed that PMJs could originate as a result of magnetic reconnection between the spine and interspine magnetic fields.

Using *Interface Region Imaging Spectrograph* (*IRIS*; De Pontieu et al. 2014) observations, Tian et al. (2014) found the presence of subarcsecond bright dots (BDs) above sunspot penumbra in the transition region (TR). They appear ubiquitously and most have a lifetime of less than a few minutes. They sometimes appear slightly elongated along the penumbral filaments and also move along the filaments with speeds of 10–40 km s^{-1}. They proposed that some of them could be due to impulsive reconnection in the TR and chromosphere at footpoints of coronal magnetic loops and others are probably due to falling plasma. It is still unclear how BDs are formed and if they show any signatures in the lower and upper atmosphere.

Vissers et al. (2015) studied the multi-wavelength signatures of PMJs and found that PMJs show a spatial offset from the chromosphere to the TR in the direction of the PMJ. Hence, they proposed that PMJs may progressively heat up to TR temperatures. Tiwari et al. (2016) could not find a noticeable signature of normal PMJs in any Atmospheric Imaging Assembly (AIA; Lemen et al. 2012) passbands, although a few strong and large PMJs show BD/BD-like signatures in the 1600 Å and High-Resolution Coronal Imager (Hi-C) 193 Å images. Alpert et al. (2016) found that BDs observed in Hi-C are slower on average, dimmer, larger in size, and longer-lived than *IRIS* penumbral BDs. They also found that most of the BDs observed in Hi-C 193 Å may correspond to TR. Deng et al. (2016) found that the locations of most of the penumbral BDs show downflow. Their statistical analysis shows that BDs do not have a consistent brightening response in the chromosphere. Following Tian et al. (2014), they also suggested that TR penumbral BDs are a manifestation of falling plasma from coronal heights along more vertical and dense magnetic loops or small-scale impulsive magnetic reconnection at TR or higher heights. Kleint et al. (2014) and Chitta et al. (2016) observed heating events that are associated with the strong downflows in the TR and proposed a similar scenario. Bai et al. (2016) have studied small transient brightening events in the penumbra and found that the penumbra shows redshifts in the Si IV 1402.77 Å line, an inward motion toward the umbra in *IRIS* 1400 Å images, and has a multi-thermal component. They proposed the triggering mechanism as magnetic reconnection at low coronal heights. A component of the plasma from the reconnection site may move downward and reach the TR, which is confirmed by

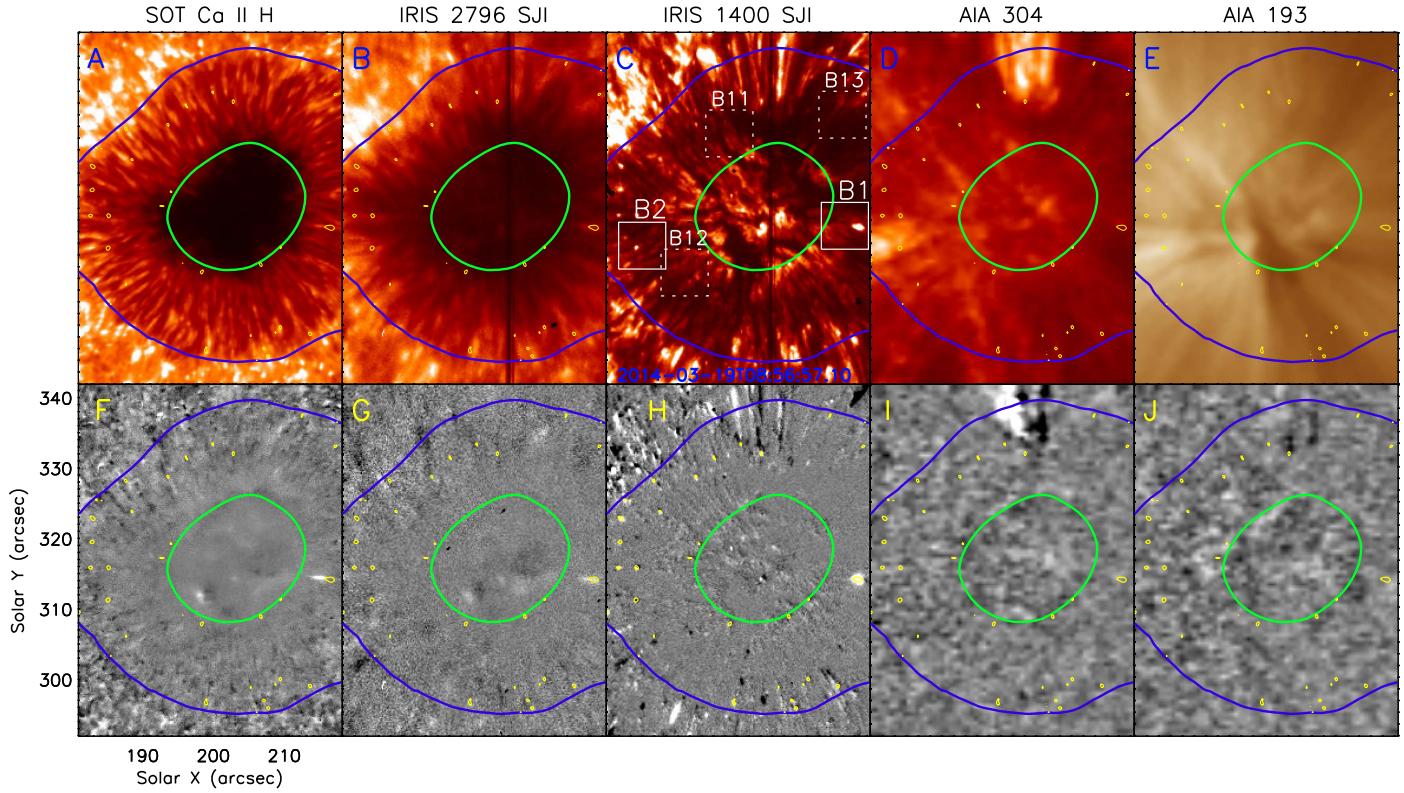

Figure 1. A–E: image of a sunspot as seen by the SOT, *IRIS*, and AIA around 08:57 UT on 2014 March 19. F–J: running difference images. The green and blue contours, derived from a time-averaged smoothed SOT image, represent the umbra and penumbra of the sunspot, respectively. The yellow contours mark the locations of bright dots (BDs). The evolutions of the BDs inside boxes B1 and B2 (as marked in the 1400 Å) are shown in Figure 2. (Animated figures corresponding to B1, B2, and B11–B13 are available.)

(Animations (a, b, c, d, e and f) of this figure are available.)

the observed redshifts in the Si IV 1402.77 Å line and the inward motions as seen in the *IRIS* 1400 Å images. Finally, it reaches the chromosphere and appears as ribbon-like brightening.

In this work, combining multi-wavelength observations covering the chromosphere and the TR/corona we try to find the source of the BDs and their relation to PMJs.

2. Data Analysis and Results

2.1. Observation and Data Reduction

We use the data obtained from a coordinated observation taken on 2014 March 19, using the *HINODE*/SOT (HOP-250; Tsuneta et al. 2008), *IRIS* (IRIS-3840007453; De Pontieu et al. 2014), and the AIA (Lemen et al. 2012) on board the Solar Dynamics Observatory. The coordinated observation between all the instruments was performed from 08:51 UT to 09:46 UT. We selected a FOV of 37″ × 50″ centered at 200″ and 317″. The FOV is limited due to the SOT observations. *IRIS* Slit-jaw images (SJI) centered at 2796 Å and 1400 Å are dominated by the Mg II k and Si IV emission lines, respectively. The SOT filter is dominated by the Ca II H line, which forms at the lower chromosphere where the temperature is below 10^4 K. The *IRIS* 2796 Å images are dominated by the emission from a plasma at temperatures of ∼10,000–15,000 K and represent the middle chromosphere. The *IRIS* 1400 Å passband is sensitive to TR ∼60,000–80,000 K. AIA filtergram images centered at 304 Å (sensitive to ∼0.05 MK) and 193 Å (∼1.25 MK) are dominated by He II and Fe XII emission lines, respectively. SOT Ca II H data were taken with 0.3 s exposure and 1.58 s cadence. *IRIS* SJIs were obtained with 4 s exposure and a cadence of 10.5 s. AIA 304 Å and 193 Å observations were taken with 2 s exposure and 12 s cadence. AIA data were then co-aligned and de-rotated to the start time (08:51 UT) of observation to compensate for the solar rotation. The pixel sizes of SOT, SJIs, and AIA are 0.″109, 0.″166, 0.″6, respectively. We have interpolated SOT and AIA data in space and time to match the *IRIS* SJI cadence (10.50 s) and spatial resolution (0.″33). The *IRIS* SJIs and SOT images were co-aligned using *IRIS* 2796 Å and SOT Ca II H images. The time difference between the SOT and *IRIS* image is of the order of subseconds. After that *IRIS* and AIA were co-aligned using *IRIS* 1400 Å and AIA 1600 Å images (Samanta et al. 2015).

Figure 1 shows the image of a sunspot, where the bottom rows (G-K) correspond to running difference images. The yellow contours show the location of BDs in the sunspot penumbra. These contours are obtained from the 1400 Å image after subtracting the same image with a 8 × 8 pixel smoothing. The evolutions of two BDs inside boxes B1 and B2 (as marked in 1400 Å) are shown in Figure 2. The BDs inside box B1, including box B11, B12, and B13, are related to PMJs. The BD inside box B2 is not related to any visible dynamics in the SOT.

2.2. Temporal Evolution of BDs and PMJs

Figure 2 depicts the temporal evolution of two BDs. (B1) shows the evolution of the BD inside the B1 box in the Figure 1. Panels A, C, and E show the evolution as seen in the *IRIS* 1400 Å, SOT Ca II H, and *IRIS* 2796 Å lines, whereas

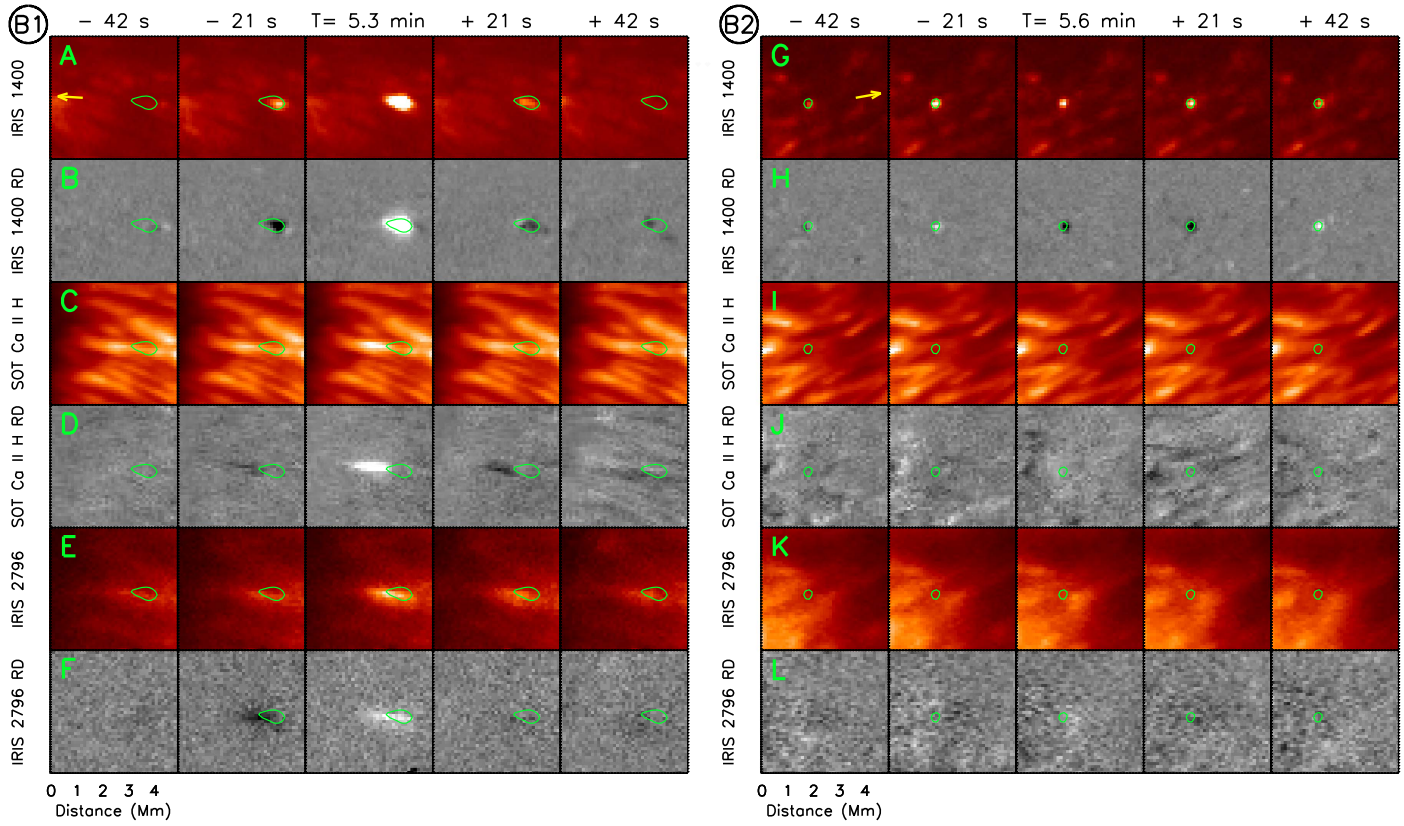

Figure 2. (B1) shows the temporal evolution of a BD and a PMJ inside the B1 region (as marked in the Figure 1) as seen in different filtergram images and their running difference images. The green contour is derived from the top middle panels to show the location of the BD. The yellow arrow indicates the direction of the sunspot center. Similarly, (B2) shows the temporal evolution of the B2 region (as marked in the Figure 1).

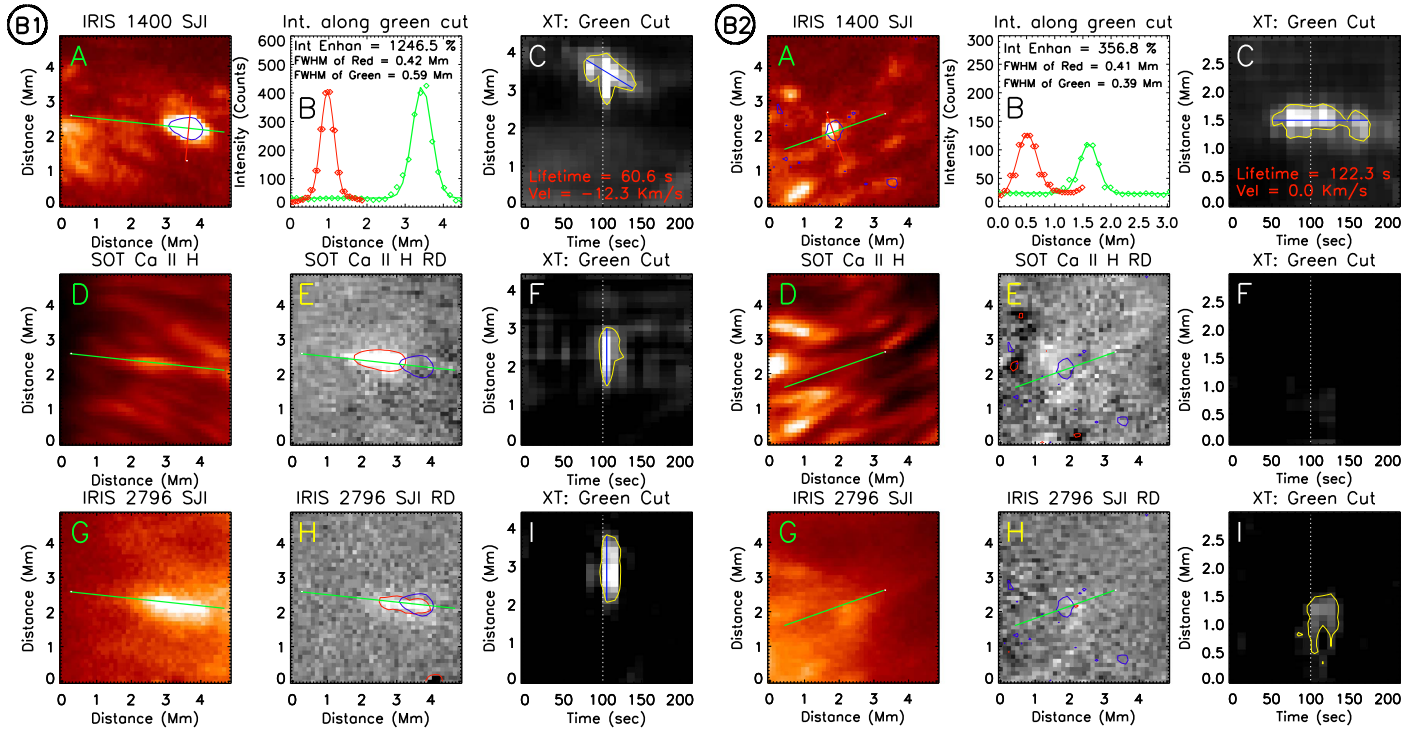

Figure 3. (B1) shows the procedure for determining the physical parameters of the BD and the PMJ inside the B1 region (as marked in the Figure 1). (A) shows the BD enclosed by the blue contour as seen in the 1400 Å. The green slit and red slit are placed along the radially outward direction and its perpendicular direction, respectively. (B) shows the intensity profile along the green and red slit with a diamond symbol. The solid line is a Gaussian fit to the profiles to determine the width and intensity enhancement of the BD. (C) shows the temporal evolution (*XT* plot) along the green cut. The yellow contour shows the region above 2σ intensity enhancement. The slop of the blue line is used to determine the plane of the sky velocity of the BD. (D) shows the Ca II H image. The green line is the slit to determine the *XT* plot. (E) shows the Ca II H image after subtracting the previous frame. The red contour shows the location of the PMJ. (F) shows the *XT* plot for the green cut of Ca II H images. (G) shows the 2796 Å image. (H)–(I) are similar to (E)–(F), respectively, but are for the 2796 Å channel. Similarly, (B2) shows the BD inside B2 region (as marked in the Figure 1).

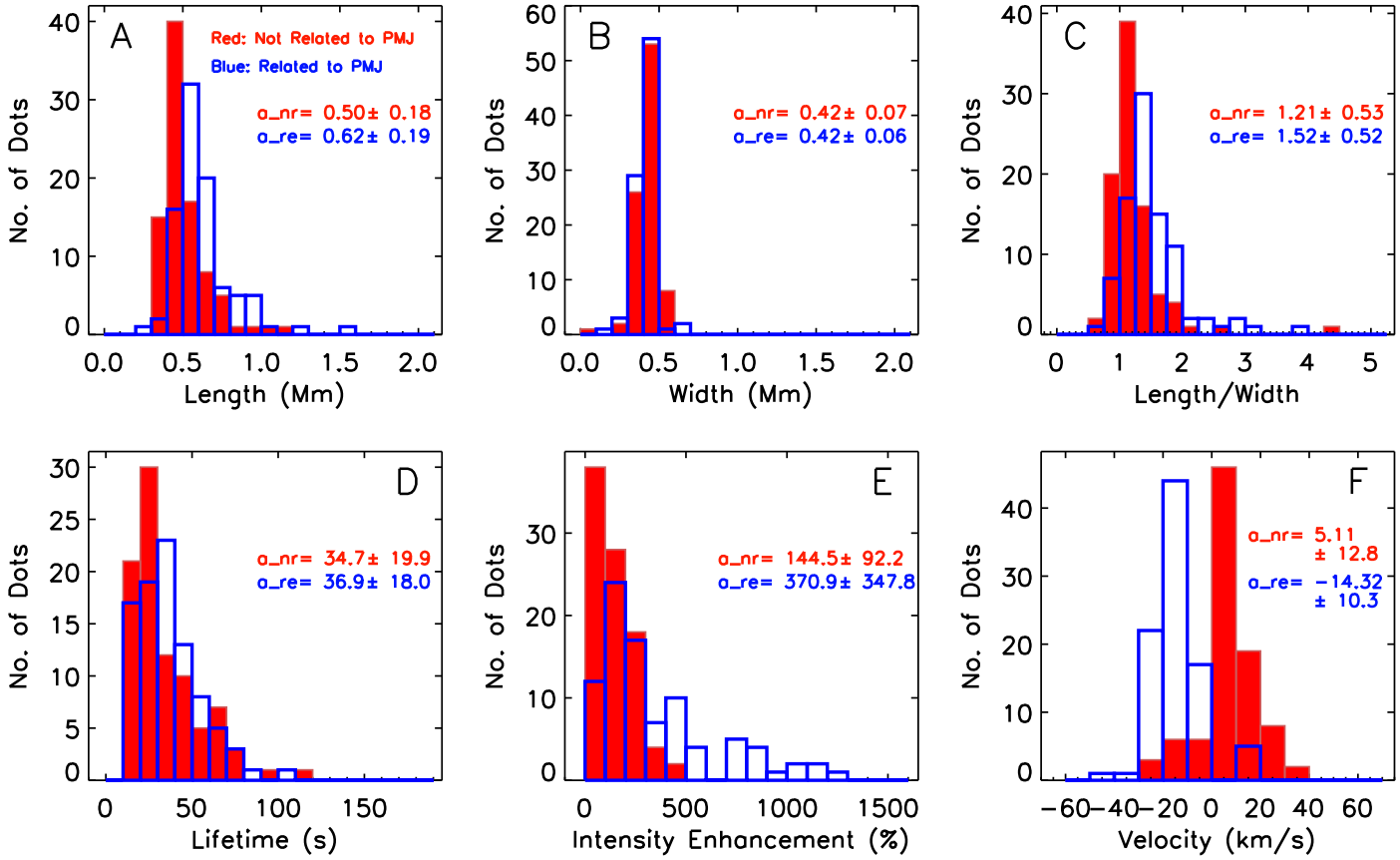

Figure 4. (A)–(F) show the distribution of different physical parameters of BDs. Red represents the BDs that do not have any connection to the PMJs, and blue represents those which are found on the top of the PMJs. (A) shows the length (FWHM of the intensity profiles along the green slit), (B) shows the width (FWHM of the intensity profiles along the red slit), (C) shows the ratio of length and width, (D) shows the lifetime, (E) shows the intensity enhancement, and (F) shows the plane of the sky speed of the BDs. The average value of each parameter and also its standard deviation are also provided (*a_nr* and *a_re*).

panels B, D, and F correspond to running difference images. The clear presence of a BD is seen in the in the 1400 Å line. A jet-like feature is also seen in the Ca II H and 2796 Å images. Similarly, ⓑ2 shows the evolution of the B2 region as marked in Figure 1. Here, we can clearly find the presence of a BD in the 1400 Å channel but no clear signature of intensity enhancement in the Ca II H. We have identified several BDs and performed a statistical analysis to compile the properties of these BDs and their signatures in the other channels. At first, we manually identify an isolated BD and look for the time frame where it shows maximum intensity enhancement. We use that as our central frame and have created a video (see the Figure 2 animation, which covers a 5 × 5 Mm region for a duration of 210 s) to follow the BDs and their direction of propagation. The BDs often show apparent movements along the bright filamentary structures roughly in the radial direction of the sunspot.

To find the properties of the BDs, we follow a similar method as used by Tian et al. (2014). Two examples of the analysis are shown in Figure 3 ⓑ1 & ⓑ2. We have studied 180 penumbral BDs and try to find if they have any signatures in the SOT Ca II H and *IRIS* 2796 Å channels. We use the central image to compute the intensity enhancement, length, and width of a BD, as shown in Figure 3 ⓑ1. We plot the intensities along the green cut and red cut (panel A). The green cut is placed along the radial direction and the red cut is perpendicular to it. The intensity values are shown by red and green diamond symbols. A fitted Gaussian is also overplotted with the same color. The FWHM of the green profile provides an estimate of the length of the BD, whereas the red profile provides the width. The percentage of intensity enhancement is calculated from the peak intensity and the linear background of the fitted Gaussian. Of the two values, the lowest value (green and red) measures the intensity enhancement. We plot a spacetime (*XT*) diagram (panel C) to study their temporal behavior and to measure their apparent speed. A 2σ intensity contour is drawn on the *XT* map. The inclined blue line is drawn inside the contour to measure the apparent velocity and lifetime of the BD. The starting time of the blue line is considered to be the initiation of the BD. The long intensity strip at the center of the *XT* map is due to high intensity enhancement at that particular time frame. We follow a similar method for the Ca II H and 2796 Å channels (D and G). The intensity enhancement in these channels is only a few percent and it is very difficult to find the location of the intensity enhancement. Thus, we use the running difference images to place our green and red cut (see E and H) on the original images. The *XT* map is produced after removing a smoothed background from each image. An elongated bright structure is seen in the *XT* plot. These have been conventionally referred as penumbral micro-jets (PMJs) by Katsukawa et al. (2007). The lifetimes of these jets are very small. Most of them appear as sudden brightening in the *XT* plot and hence it is very difficult to determine their direction of propagation and the speed. In this work we do not focus on the

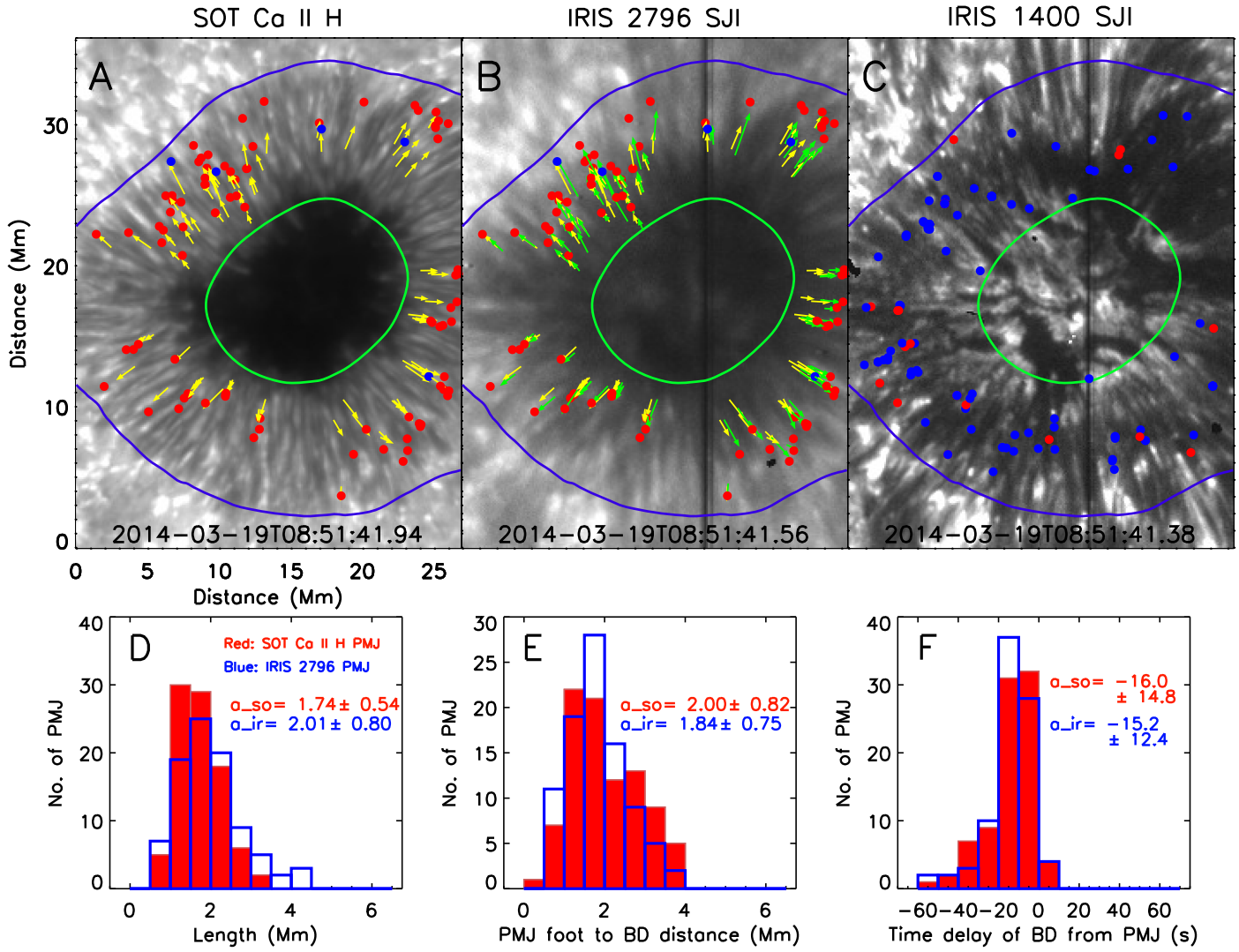

Figure 5. (A): The yellow arrows show the location of the PMJs as found in the Ca II H images and the dots (red/blue) show the location of the BDs as seen in the 1400 Å channels over the Ca II H image. Red dots represent the BDs that move in an inward direction (opposite of the PMJ's direction) and blue represents the BDs that move outward (along the direction of PMJs). (B): The yellow arrow and the dots (red/blue) show the location of Ca II H PMJs and 1400 Å BDs over the 2796 Å SJI. The green arrows represent the PMJs as observed in the 2796 Å images. (C): The BDs that do not have any visible counterparts in the Ca II H images are shown over the 1400 Å image. (D): The distribution of the length of the PMJs. (E): The distribution of the distance between the footpoint of the PMJs and starting location of the BDs. (F): the distribution of the time delay of the origination of BDs after PMJ. A negative value means that a BD originates earlier than a PMJ. All the PMJs and BDs are observed over the total observing window, whereas the background images are taken at t = 0. The mean values of each parameter and also their standard deviations are printed. The *a_so* and *a_ir* represent the mean value as obtained from the SOT Ca II H and *IRIS* 2796 Å, respectively.

speed of these jets. Using earlier conventions we have assumed that these brightenings are propagating outward from the sunspot, though it is not clearly established from our analysis that the bright structures are moving outward from the sunspot. We use a 2σ intensity contour to find the location and extent of the PMJ. The blue line is drawn along the direction of intensity enhancement. The starting time of the blue line is considered as the initiation and the length of the line is considered as the length of the PMJ. We can clearly see that the BD appears before the PMJ in this example.

Similarly, in Figure 3(R2), we study another BD. Following the same methodology we study the evolution of the BD. We could not find a clear signature of the BD in the Ca II H, though a faint signature is seen in the 2796 Å channel. In the following subsection a statistical study is performed to find out if there are two types of BDs present in our data.

2.3. Statistical Behavior of the BDs

We analyze the properties of many BDs and their signatures in the other channels. Out 180 total events, 90 are identified as having a correlated signature in the Ca II H and 2796 Å channels, while the other 90 do not. We have separated these two classes to find out if they have any significant differences in their physical properties. Figures 4(A)–(F) show the distributions of the observed parameters. The red color in the histograms represents the BDs that do not have a counterpart in the Ca II H images, whereas the blue represents the BDs that are related to the Ca II H PMJs. The mean value of each of the parameters for both types is also provided. We find that the BDs that are related to PMJs are generally longer and have higher intensity enhancements. They are also more elongated (the ratio between length and width is higher). One of the

distinguishable features is that most of the BDs that are related to PMJs show negative velocities (drifts toward the center of the sunspot).

2.4. Statistical Behavior of PMJs and Their Connection to BDs

We have also calculated a few physical parameters of PMJs. The positions and lengths of the PMJs are measured in both the 2796 Å and Ca II H channels. The starting point of the PMJs is considered to be the location close to the center of the sunspot. The locations of the PMJ as seen in the Ca II H and 2796 Å channels are marked (yellow arrows) in Figures 5(A) and (B), respectively. The length of the arrow measures the length of the PMJs. The BDs that are related to these PMJs are also shown by the small dots. Red represents the dots that move inward and blue represents those that move outward from the sunspot center. The PMJs as seen in 2796 Å generally show a spatial offset from the Ca II H PMJs along the PMJ direction (outer penumbral side). In Figure 5(C) we show the location of the BDs that are not related to any PMJs. Figure 5(D) shows the distribution of the length of the PMJs as seen in the 2796 Å and Ca II H images. The PMJs in Ca II H have similar values, as reported by Katsukawa et al. (2007), though they appear to be a little longer in the 2796 Å images. Figure 5(E) shows the distribution of the length between the BDs and the footpoint of the PMJs and Figure 5(F) shows the time delay between the appearance of the BDs and PMJs. A negative value means that BDs appear earlier than the PMJs. We find that most of the BDs appear before the PMJs.

3. Summary

We have analyzed the properties of 180 BDs as seen in the 1400 Å images above a sunspot. Using our coordinated observations, we have also positively identified PMJs in the SOT Ca II H and *IRIS* 2796 Å images. We find that 90 BDs are related to PMJs, whereas others are not. A detailed analysis shows that the BDs that are related are generally longer and more elongated and have higher intensity enhancements. Most of these BDs show negative velocities (move in an inward direction) and appear at the top of the PMJs. These BDs are found to appear before the generation of the PMJs. These results may indicate that BDs could originate from a magnetic reconnection occurring at low coronal heights and/or be due to falling plasma. A component of the plasma from the reconnection site may move downward and reach the TR and show inward motion, as seen in the *IRIS* 1400 Å images. Finally, it reaches the chromosphere and appears as ribbon-like brightening (PMJ), which could explain the time delay in the appearance of the PMJs and their short lifetimes. Klimchuk (2006), Jiang et al. (2012), and Winebarger et al. (2013) proposed that this kind of small magnetic reconnection occurs in the low corona. This is in contrast to the reconnection model as proposed by Katsukawa et al. (2007). The progressive heating mechanism of the PMJs as proposed by Vissers et al. (2015) also may not explain the inward motions of the BDs, the appearance of BDs before PMJs, and the longer lifetime of the BDs. It is still unclear how the non-related BDs originate.

We thank Yukio Katsukawa for useful discussions and suggestions. H.T. is supported by the Recruitment Program of Global Experts of China, NSFC under grant 41574166, and the Max Planck Partner Group program. H.T. thanks ISSI Bern for the support to the team "Solar UV bursts—a new insight to magnetic reconnection." We thank the *Hinode*, *IRIS*, and *SDO* teams for providing the data in the public domain. *Hinode* is a Japanese mission developed and launched by ISAS/JAXA, with NAOJ as domestic partner and NASA and STFC (UK) as international partners. It is operated by these agencies in co-operation with ESA and NSC (Norway). *IRIS* is a NASA small explorer mission developed and operated by LMSAL with mission operations executed at NASA Ames Research center and major contributions to downlink communications funded by ESA and the Norwegian Space Centre.

References

Alpert, S. E., Tiwari, S. K., Moore, R. L., Winebarger, A. R., & Savage, S. L. 2016, ApJ, 822, 35
Bai, X. Y., Su, J. T., Cao, W. D., et al. 2016, ApJ, 823, 60
Bellot Rubio, L. R., Balthasar, H., & Collados, M. 2004, A&A, 427, 319
Chitta, L. P., Peter, H., & Young, P. R. 2016, A&A, 587, A20
De Pontieu, B., Title, A. M., Lemen, J. R., et al. 2014, SoPh, 289, 2733
Deng, N., Yurchyshyn, V., Tian, H., et al. 2016, ApJ, 829, 103
Henriques, V. M. J., & Kiselman, D. 2013, A&A, 557, A5
Jiang, R.-L., Fang, C., & Chen, P.-F. 2012, ApJ, 751, 152
Katsukawa, Y., Berger, T. E., Ichimoto, K., et al. 2007, Sci, 318, 1594
Kleint, L., Antolin, P., Tian, H., et al. 2014, ApJL, 789, L42
Klimchuk, J. A. 2006, SoPh, 234, 41
Lemen, J. R., Title, A. M., Akin, D. J., et al. 2012, SoPh, 275, 17
Lites, B. W., Elmore, D. F., Seagraves, P., & Skumanich, A. P. 1993, ApJ, 418, 928
Samanta, T., Banerjee, D., & Tian, H. 2015, ApJ, 806, 172
Scharmer, G. B., & Henriques, V. M. J. 2012, A&A, 540, A19
Scharmer, G. B., Henriques, V. M. J., Kiselman, D., & de la Cruz Rodríguez, J. 2011, Sci, 333, 316
Tian, H., Kleint, L., Peter, H., et al. 2014, ApJL, 790, L29
Tiwari, S. K., Moore, R. L., Winebarger, A. R., & Alpert, S. E. 2016, ApJ, 816, 92
Tiwari, S. K., van Noort, M., Lagg, A., & Solanki, S. K. 2013, A&A, 557, A25
Tiwari, S. K., van Noort, M., Solanki, S. K., & Lagg, A. 2015, A&A, 583, A119
Tsuneta, S., Ichimoto, K., Katsukawa, Y., et al. 2008, SoPh, 249, 167
Vissers, G. J. M., Rouppe van der Voort, L. H. M., & Carlsson, M. 2015, ApJL, 811, L33
Winebarger, A. R., Walsh, R. W., Moore, R., et al. 2013, ApJ, 771, 21